

2D1-3

# Ground Wave Propagation on Mixed-Paths through Urban Areas

Toru Kawano, Keiji Goto, and <sup>#</sup>Toyohiko Ishihara

Department of Communication Engineering, National Defense Academy

Hashirimizu 1-10-20, Yokosuka, 239-8686 Japan, Tel: +81-46-841-3810

Fax: +81-46-844-5903, E-mail: ishihara@cc.nda.ac.jp

## 1. Introduction

Medium-frequency (MF) ground wave propagation is playing one of the most important roles for a long distance communication. When the surface impedance of the earth along the propagation path changes the ground wave propagation is influenced strongly as it occurs when the radio wave traverses a border from an urban area to a suburban area or viceversa [1]-[4]. The measurements of the ground wave propagation in the urban areas have shown the unexpected high attenuation in some parts of cities and the anomalous variation pattern of the field strength with distance [2], [5]-[9].

In this paper, we shall examine both experimentally and theoretically the ground wave propagation over the mixed-paths which traverse first the open area along which one can see the transmitting antenna, then the built up area along which the density of the man-made objects is very high, and finally the medium density area. We will show that the experimental results, obtained in the measurements performed in Kanto area including the city of Tokyo in Japan, agree very well with the three-section mixed-path theory [1], [3], [4], [7]-[9].

## 2. Three-Section Mixed-Path Theory with Tropospheric Ducting Effect

In this section, the ground wave propagation over a three-section mixed-path as shown in Fig.1 is considered. In Fig.1(a), we have shown a  $(x, \phi, v)$  coordinate system and a three-section mixed-path consisting of the surface impedances  $Z_a$  ( $-\infty \leq x < \ell_a$ ),  $Z_b$  ( $\ell_a \leq x < \ell_b$ ), and  $Z_c$  ( $\ell_b \leq x < \infty$ ). A vertical transmitting antenna T and a vertical receiving antenna R are placed on the surface with the impedance  $Z_a$  and on the surface with the impedance  $Z_c$ , respectively. While, Fig. 1(b) shows the tropospheric surface duct with the modified refractive index  $m(v)$  defined by  $m(v) = n(v) + v/a \approx 1 - v/a_0$ ,  $n(v) = (\varepsilon_r(v))^{1/2}$ . Here,  $a$  denotes the radius of curvature of the earth,  $n(v)$  and  $\varepsilon_r(v)$  are the refractive index and the relative dielectric constant at the height  $v$ , and  $-a_0^{-1}$  is the equivalent duct parameter indicating the strength of the surface duct.

When the current  $I$  is given on the antenna T whose length is  $ds$ , the vertical electric field  $E_v$  observed at the vertical receiving antenna R located at  $(x = \ell, v = 0)$  may be represented as follows [1], [3], [7]-[9].

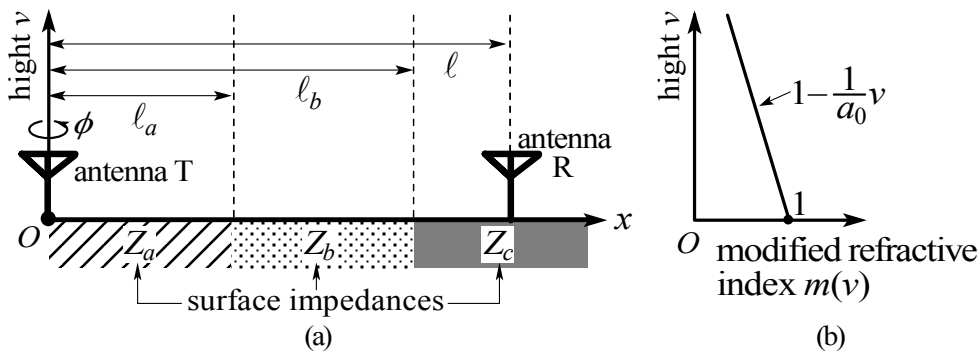


Figure 1(a): Coordinate system  $(x, \phi, v)$  and three-section mixed-path consisting of surface impedance  $Z_a$ ,  $Z_b$ , and  $Z_c$ , and (b): modified refractive index.

$$E = E_0 W(\ell, Z_a, Z_b, Z_c), \quad E_0 = -i\omega\mu_0\varepsilon_r(0)Ids \frac{\exp(i k \ell)}{2\pi\ell} \quad (1)$$

$$\begin{aligned} W(\ell, Z_a, Z_b, Z_c) &= W(\ell, Z_a) - \left( \frac{-ik\ell}{2\pi} \right)^{1/2} \frac{Z_c - Z_a}{Z_0} \int_{\ell_2}^{\ell} \frac{W(x, Z_a) W(\ell - x, Z_c)}{\sqrt{x(\ell - x)}} dx \\ &\quad - \left( \frac{-ik\ell}{2\pi} \right)^{1/2} \frac{Z_b - Z_a}{Z_0} \int_{\ell_1}^{\ell_2} \frac{W(x, Z_a) \tilde{W}(x, Z_b, Z_c)}{\sqrt{x(\ell - x)}} dx \end{aligned} \quad (2)$$

Where  $W(\ell, Z_a)$  in (2) denotes the attenuation function over the homogenous surface impedance  $Z_a$  defined by [6], [7], [9], [10]

$$\begin{aligned} W(\ell, Z_a) &= F(\rho) - \frac{1}{2} \left\{ (1 + 2\rho)F(\rho) - 1 - i\sqrt{\pi\rho} \right\} \delta^3 \\ &\quad + \left\{ \left( \frac{\rho^2}{2} - 1 \right) F(\rho) + i\sqrt{\pi\rho} (1 - \rho) + 1 - 2\rho + \frac{5}{6}\rho^2 \right\} \delta^6 + \dots, \end{aligned} \quad (3)$$

$$F(\rho) = 1 + i\sqrt{\pi\rho} \exp(-\rho) \operatorname{erfc}(-i\rho^{1/2}), \quad \rho = ik\ell Z'^2 / 2, \quad (3a)$$

$$\delta = i2^{-1/3} / \{(ka_0/2)^{1/3} Z'\}, \quad Z' = Z_a/Z_0, \quad Z_0 = \sqrt{\mu_0/\varepsilon(0)}, \quad (3b)$$

while, the attenuation function  $\tilde{W}(x, Z_b, Z_c)$  in (2) is defined by

$$\begin{aligned} \tilde{W}(x, Z_b, Z_c) &= W(\ell - x, Z_c) - \left( \frac{-ik(\ell - x)}{2\pi} \right)^{1/2} \frac{Z_b - Z_c}{Z_0} \\ &\quad \cdot \int_x^{\ell_2} \frac{W(x' - x + \ell - \ell_2, Z_c) W(\ell_2 - x', Z_b)}{\sqrt{(\ell_2 - x')(x' - x + \ell - \ell_2)}} dx'. \end{aligned} \quad (4)$$

Note that when the atmosphere is homogenous, i.e., when  $a_0 \rightarrow \infty$  (see Fig. 1(b)), the duct parameter  $\delta$  defined in (3b) becomes  $\delta = 0$ . In this case, the attenuation function  $W(\ell, Z_a)$  is represented by the Sommerfeld function  $F(\rho)$ . When the conditions  $-45^\circ < \arg Z' < 90^\circ$ ,  $|\rho| \gg 1$  are satisfied, the Sommerfeld functions  $F(\rho)$  defined in (3a) can be expanded as

$$F(\rho) = F_g(\rho) = -\frac{1}{2\rho} - \frac{1 \cdot 3}{(2\rho)^2} - \frac{1 \cdot 3 \cdot 5}{(2\rho)^3} - \frac{1 \cdot 3 \cdot 5 \cdot 7}{(2\rho)^4} - \frac{1 \cdot 3 \cdot 5 \cdot 7 \cdot 9}{(2\rho)^5} \dots \quad (5a)$$

While when the conditions  $-90^\circ < \arg Z' < -45^\circ$ ,  $|\rho| \gg 1$  are satisfied, which correspond to a highly inductive conditions,  $F(\rho)$  can be expressed by

$$F(\rho) = F_g(\rho) + 2i\sqrt{\pi\rho} e^{-\rho} \quad (5b)$$

The Sommerfeld function  $F(\rho)$  in (5a) and (5b) will be used in the theoretical calculation in the Sec. 3.

### 3. Experimental Results and Comparison with Theoretical Results

We will compare the experimental results performed in Tokyo and Kanagawa areas in Japan with the theoretical results calculated from the solutions derived in the previous section. The measurements have been performed along the routes I and II shown in Fig. 2. The two routes I and II traverse first the open area then the high density urban area and finally the medium density urban area. Therefore the three-section mixed-path theory described in the Sec. 2 can be used in the theoretical calculation.

Fig. 3 shows the experimental result (●●●) and the theoretical result (—: solid curve) along the route I. On the route I, the land  $a$  between 0 km and 7 km ( $0 \text{ km} < \ell < 7 \text{ km}$ ) corresponds to the open area, the land  $b$  from 7 km to 20 km ( $7 \text{ km} < \ell < 20 \text{ km}$ ) corresponds to the high density urban

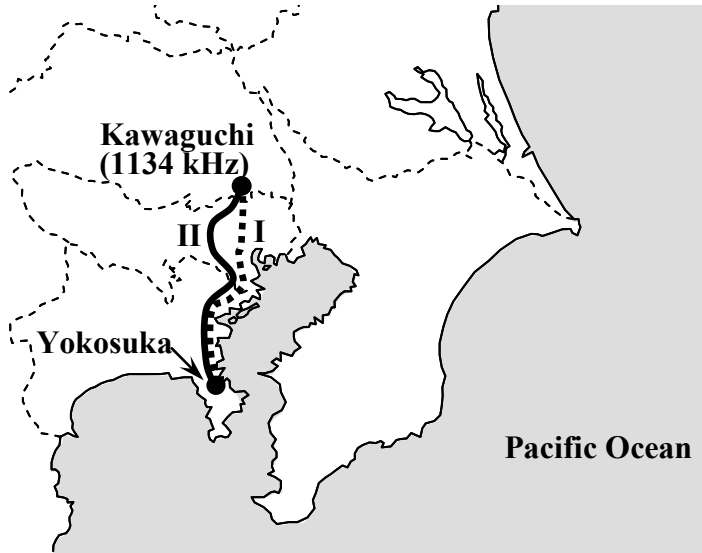


Figure 2: Routes I and II in Tokyo and Kanagawa, Japan used in the experiment.

area, and the land  $c$  from 20 km to 60 km the medium density area. The surface impedances  $Z_a = 0.079Z_0\exp(-i43^\circ)$ ,  $Z_b = 0.27Z_0\exp(-i78^\circ)$ , and  $Z_c = 0.18Z_0\exp(-i76^\circ)$  are used in the calculations along the land  $a$ , land  $b$ , and land  $c$ , respectively (Note that  $Z_0 (= \sqrt{\mu_0 / \epsilon_0})$  denotes the characteristic impedance in the air). The surface impedance  $Z_b$  satisfies the highly inductive conditions and the surface impedance  $Z_c$  satisfies the inductive conditions. Therefore, in the propagation along the land  $b$  and the land  $c$ , the slow-wave type surface wave can be excited in addition to the conventional Norton ground wave [6]-[9], [11]. The theoretical result (—) calculated from the three-section mixed-path theory given in the Sec. 2 agrees very well with the measurements (●●●). The dotted curve (---) shown in Fig. 3 shows the theoretical result on the homogeneous surface impedance with the impedance  $Z_s = 0.079Z_0\exp(-i43^\circ)$ . The electric field magnitude decreases monotonically as the function of the distance  $\ell$ . By comparing with the theoretical result for the ground wave propagation along the homogeneous surface impedance, it is observed that the electric field magnitude along the route I shows the unexpected high attenuation in the region between  $10 \text{ km} \leq \ell \leq 60 \text{ km}$ , and the anomalous oscillation pattern of the field magnitude with the distance  $\ell$ . These unexpected and anomalous phenomena can be explained as the result of the interference between the Norton ground wave and the slow-wave type surface wave [6]-[9].

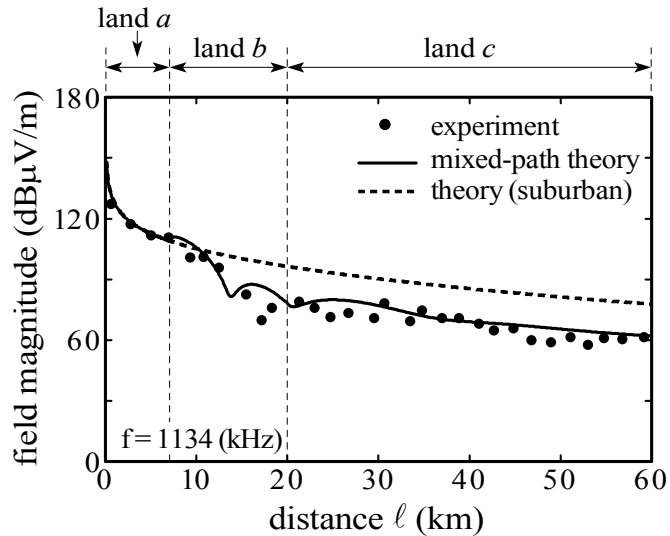


Figure 3: Ground wave propagation along the route I on three-section mixed-path.

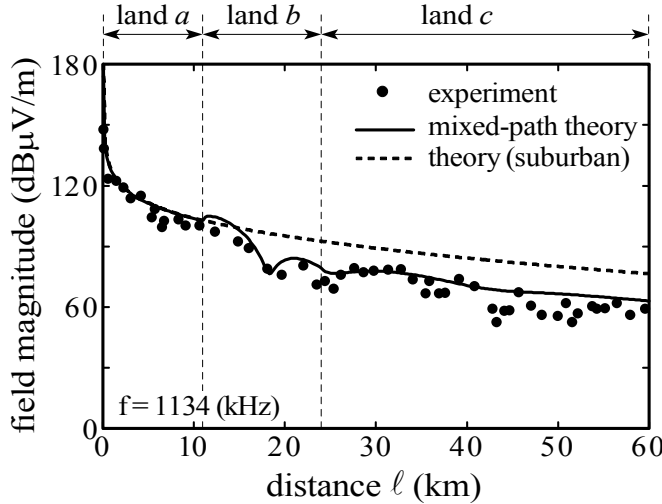


Figure 4: Ground wave propagation along the route II on three-section mixed-path.

Fig. 4 shows the ground wave propagation along the route II. We have chosen the different route from the route I in the region  $0 \text{ km} \leq \ell \leq 40 \text{ km}$  in the measurements along the route II. In the region  $40 \text{ km} \leq \ell \leq 60 \text{ km}$ , the routes I and II are almost the same. As shown in Fig. 4, the experimental results ( $\bullet\bullet\bullet$ ) agree also very well with the three-section mixed-path theory (—). Note that we have used  $Z_a = 0.079Z_0\exp(-i43^\circ)$ ,  $Z_b = 0.255Z_0\exp(-i78.6^\circ)$ , and  $Z_c = 0.17Z_0\exp(-i77.8^\circ)$  in the calculation. Through the measurements along the route II, one may confirm the high attenuation and the anomalous variation with distance of the electric field magnitude.

## 4. Conclusion

We have performed the measurements of the MF (Medium Frequency) ground wave propagation in the Kanto area in Japan and compared the experimental results with the theoretical results calculated from the three-section mixed-path theory. We have shown that the measured results agree very well with the three-section mixed-path theory. It is shown that the surface impedance in the urban area can be characterized by a highly inductive surface impedance which can support the slow-wave type surface wave in addition to the Norton ground wave. The electric field magnitude shows the unexpected attenuation and the anomalous oscillation with distance due to the interference between the Norton ground wave and the slow-wave type surface wave.

## References

- [1] K. Furutsu, Journal of the Radio Research Laboratories, vol. 2, no. 10, pp. 345-398, Oct. 1955.
- [2] J. H. Causebrook, Proc. IEE, vol. 125, no. 9, pp. 804-808, Sept. 1978.
- [3] J. R. Wait, IEEE Antennas and Propagation Magazine, vol. 40, no. 5, pp. 7-24, Oct. 1998.
- [4] L. Sevgi and L. B. Felsen, Int. Journal of Numer. Model. : Electronic Networks, Devices and Fields, vol. 11, pp. 87-103, Nov. 1998.
- [5] T. Ishihara and Y. Mukai, Proceedings of 1996 International Symposium on Antennas and Propagation (ISAP '96), Chiba, Japan, pp. 297-300, Sep. 1996.
- [6] T. Kawano and T. Ishihara, IEEE AP-S Int. Symp. Digest, vol. 1A, pp. 375-378, Washington D. C., USA, July 2005.
- [7] T. Kawano and T. Ishihara, IEEE AP-S Int. Symp. Digest, vol. 5, pp. 4735-4738, Albuquerque, USA, July 2006.
- [8] T. Kawano, T. Ishihara, and K. Goto, Proceedings of 2006 International Symposium on Antennas and Propagation (ISAP 2006), Orchard Hotel, Singapore, ISBN 81-903170-8-3, Nov. 2006.
- [9] T. Kawano, K. Goto, and T. Ishihara, Trans. on IEICE, vol. E90-C, no. 2, pp. 288-294, Feb. 2007
- [10] H. Bremmer, IRE Trans. Antennas & Propag. AP-6, no. 3, pp. 267-272, 1958.
- [11] R. J. King and G. A. Schlak, Radio Science, vol. 2, no. 7, pp. 687-693, July 1967.